 doi:10.20944/preprints202209.0359.v1

Article

Modeling Patient-Specific CAR-T Cell Dynamics: Multiphasic Kinetics Via Phenotypic Differentiation

Emanuelle A. Paixão [1], Luciana R. C. Barros [2], Artur C. Fassoni [3], and Regina C. Almeida [4]

[1] Graduate Program, Laboratório Nacional de Computação Científica, Petrópolis 25651-075, Brazil; earantes@lncc.br
[2] Center for Translational Research in Oncology, Instituto do Câncer do Estado de São Paulo, Hospital das Clínicas da Faculdade de Medicina da Universidade de São Paulo, São Paulo 01246-000, Brazil; luciana.rcbarros@hc.fm.usp.br
[3] Institute for Mathematics and Computer Science, Universidade Federal de Itajubá, Itajubá 37500-903, Brazil; fassoni@unifei.edu.br
[4] Computational Modeling Department, Laboratório Nacional de Computação Científica, Petrópolis 25651-075, Brazil; rcca@lncc.br
* Correspondence: earantes@lncc.br

Simple Summary: We present the first mathematical model to describe the multiphasic dynamical treatment response in CAR-T cell kinetics through the differentiation of functional (distributed and effector), memory, and exhausted phenotypes, integrated with the dynamics of cancer cells. The CAR-T cell kinetics are evaluated for various hematologic cancers and therapy outcomes, providing insights into promising parameters for long-term therapy investigation.

Abstract: Chimeric Antigen Receptor (CAR)-T cell immunotherapy revolutionized cancer treatment and consists of the genetic modification of T lymphocytes with a CAR gene, aiming to increase their ability to recognize and kill antigen-specific tumor cells. The dynamics of CAR-T cell responses in patients presents a multiphasic kinetics with distribution, expansion, contraction, and persistence phases. The characteristics and duration of each phase depend on the tumor type, the infused product, and on patient-specific characteristics. We present a mathematical model which describes the multiphasic CAR-T cell dynamics resulting from the interplay between CAR-T and tumor cells, considering patient and product heterogeneities. The CAR-T cell population is divided into functional (distributed and effector), memory, and exhausted CAR-T cell phenotypes. The model is able to describe the diversity of CAR-T cell dynamic behaviors in different patients and hematological cancers as well as their therapy outcomes. Our results indicate that the joint assessment of the area under the concentration-time curve in the first 28 days and the corresponding fraction of non-exhausted CAR-T cells may be considered as potential markers to classify therapy responses. Overall, the analysis of different CAR-T cell phenotypes can be a key aspect for a better understanding of the whole CAR-T cell dynamics.

Keywords: Hematological malignancies; treatment outcomes; CAR-T cell exhaustion; memory pool, functional CAR-T cells; antigen dependent CAR-T expansion

1. Introduction

Chimeric antigen receptor (CAR)-T cell immunotherapy is approved by US Food and Drug Administration to treat several hematological cancers as B-cell acute lymphoblastic leukemia (ALL), multiple myeloma, mantle cell lymphoma (MCL), diffuse large B cell lymphoma (DLBCL), high-grade B cell lymphoma, primary mediastinal large B cell lymphoma, and follicular lymphoma. Although several malignancies are treated, only two antigens are targeted: CD19 and BCMA (B cell maturation antigen) [1]. All the approved therapies consist of *in vitro* insertion of a CAR gene on autologous T lymphocytes after failure of prior therapies, such as chemotherapy or HST transplantation. In a

 doi:10.20944/preprints202209.0359.v1

recent review, Huang *et al.* [2] compare CAR-T therapies approved to date, highlighting their main features.

CAR-T cells promote potent anti-leukemic activity in children and young adults against chemotherapy-resistant B-ALL [3,4]. In a follow-up study, Lee *et al.* [3] correlate complete response to therapy with greater *in vivo* expansion of CAR-T cells and recorded the median overall survival of 10.5 months for the entire cohort [4]. Melenhorst *et al.* [5] report two cases of patients with CLL who experience complete remission response for ten years. These studies highlight the capacity of CAR-T cells to induce long-term sustained response in patients. On the other hand, Gardner *et al.* [6] reported the existence of patients with longer detection of circulating CAR-T cells, but with a constant tumor burden, thus characterizing the presence of non-functional CAR-T cells. This provides evidence of a progressive loss of functionality, expansion capacity, and persistence of the CAR-T cells due to the emergence of exhausted CAR-T cell phenotype [7].

The success of CAR-T cell immunotherapy mostly depends on the patient's T lymphocytes characteristics after CAR-T cell manufacture, such as expansion, persistence, and cytotoxic capacity [8]. Thus, one of the main goals to obtain improved treatment response is avoiding or delaying T cell exhaustion and maintaining the memory phenotype [9]. Exhausted CAR-T cells are known to affect therapy response in pre-clinical studies; to overcome this issue, several strategies on CAR design and *in vitro* expansion techniques are under investigation [10]. Improvements in CAR design to develop a CAR-T cell exhaustion-resistant phenotype have shown promising results, leading to cell phenotypes with superior antitumor functions and prolonged lifespan [7]. Clinical studies show that there is a correlation between the amount of memory cells in the product with a greater CAR-T cell persistence, longer time for disease progression, and sustained remission [11]. Therefore, an analysis of T cell subsets in both the final product and the *in vivo* samples post infusion may improve the understanding of how immunophenotypes enhance the effectiveness of CAR-T cell therapy [12].

Much effort has been carried out in order to better understand the intrinsic mechanisms that regulate CAR-T immunotherapy, aiming to improve it, expand it to other types of cancers, and increase its success rates. Previous chemotherapy regimens, cytokines used to expand CAR-T cells *in vitro*, the number of CD3+ cells before apheresis, and even the CAR design (costimulatory domains and affinity to antigen) affect CAR-T cell product and the therapy success [8]. Different response to therapy profiles are observed in patients: non-response, antigen-negative relapse, antigen-positive relapse, and complete and sustained remission [3,4,13,14]. Dysfunctional CAR-T cells are to blame for non-responses and antigen-positive relapses [15], but the mechanisms associated with loss of functionality deserve more investigation.

In recent years, quantitative models have been developed to depict CAR-T cell kinetics and their interactions with cancer cells. Recent reviews have examined CAR-T structure, physicochemical and pharmacological properties, among other aspects of CAR-T cell immunotherapy [2,12,16–18]. They have also analyzed existing quantitative modeling approaches, discussing their usefulness, limitations, and challenges. Unlike traditional drugs, CAR-T cell dynamics does not follow the typical path of absorption, distribution, metalolism/catabolism, and excretion. CAR-T cells are living drugs and display unique cellular kinetic profiles [18,19]. Their characteristics encompass antigen-dependent expansion, heterogeneity of the infused product, and influence of the tumor microenvironment.

It is known that the total number of CAR-T cells circulating in peripheral blood (PB) presents a multiphasic dynamic. The first detailed analysis characterizing *in vivo* CAR-T cell kinetics across multiple diseases (ALL and CLL) was performed in [20]. In general, after the infusion, the circulating CAR-T cells decline due to the distribution of cells throughout the PB, bone marrow (BM), and other tissues. The distribution period is followed by a rapid expansion until reaching a peak, then followed by a biphasic decline in CAR-T cell numbers. In this way, the *in vivo* CAR-T cell kinetics profile is

 doi:10.20944/preprints202209.0359.v1

basically described by the expansion and persistence phases, with the latter indicating the duration of CAR-T cells in the PB and tissues [20]. The dynamics after the peak was further divided into the contraction and persistence phases in [21]. In a first mixed-effect model, Stein *et al.* [21] independently model these two phases. The contraction phase is described by a fast decline due to the programmed cell death of activated CAR-T cells and the loss of antigen stimulation. The persistence phase presents a slower decline owing to the memory phenotype, which may persist for years or decades. Correlating CAR-T cell kinetics with therapy response profile and tumor types, Liu *et al.* [22] found that responding patients exhibit, on average, higher cell expansion rate (and capacity) than non-responding patients, but a lower contraction rate. These two models [21,22] are characterized by the use of empirical piecewise functions and require the explicit definition of the timepoints that separate the phases. Also with a modeling approach, Mueller *et al.* [20] investigated the interplay among different phenotypes of CAR-T cells, including naïve, central memory, effector memory, and terminally differentiated effector, and $CD19^+$ tumor cells. Although the estimation of the model parameters was challenging, including issues such as lack of identifiability, the model allowed identifying factors related to the interindividual variability in the used clinical dataset. By modeling both *in vitro* and *in vivo* dynamics of anti-BCMA CAR-T cell therapy, Singh *et al.* [23] described the multiphasic CAR-T cell kinetics assuming that CAR-T cells are split into effector and memory populations. The authors have also investigated CAR affinity and antigen-dependent CAR-T cell expansion in a previous work [24]. Several other biological mechanisms have also been investigated in recent works, including competition between CAR-T cells and normal T cells and the role of stochastic extinction [25], the importance of lymphodepletion before applying CAR-T cell therapy [26], the interplay of proinflammatory cytokines [27], among others. Although these models could represent the total CAR-T cell dynamics, they did not focus on the interplay among different CAR-T cell phenotypes and their relation to multiphasic dynamics.

In a previous work, we modeled the dynamics of two CAR-T cell phenotypes, effector and memory CAR-T cells, in a pre-clinical model of hematological cancers [28]. Here, we extend our previous model to describe the CAR-T immunotherapy for hematological cancers in patients, considering different CAR-T cell phenotypes, including engraftment of functional CAR-T cells, memory CAR-T cells which can be converted to the effector phenotype, and loss of functional capacity when converted to exhausted CAR-T cells. To our knowledge, this is the first model in the literature which considers the multiphasic dynamics of CAR-T cell kinetics through the differentiation of functional, memory, and exhausted phenotypes, integrated with the dynamics of cancer cells in a single model. *In vivo* CAR-T expansion is considered time-dependent and modulated by the antigen expression. Several individual patients' characteristics, such as the CAR-T cell expansion capacity and persistence duration, are incorporated into the model. By fitting the model to patients with different types of hematologic cancers and therapy outcomes, we analyze and evaluate the influence of phenotypic differentiation on the dynamics and several kinetic parameters to identify those that best characterize long-term responses.

2. Methods

We present a mathematical model to describe the response of CAR-T cell immunotherapy against B-cell malignancies in patients, as schematically described in Figure 1. The model extends the one presented in [28], which was developed for pre-clinical scenarios with immunodeficient mice. Here, the main feature is the multiphasic CAR-T cell dynamic, characterized by (i) the distribution of CAR-T cells in the patient's body right after infusion, (ii) a quick expansion phase, followed by (iii) a contraction phase of the cell population, and (iv) a long-lasting CAR-T cell persistence. The suggested multiphasic CAR-T cell dynamics is sketched in Figure 1a.

Preprints (www.preprints.org) | NOT PEER-REVIEWED | Posted: 23 September 2022 doi:10.20944/preprints202209.0359.v1

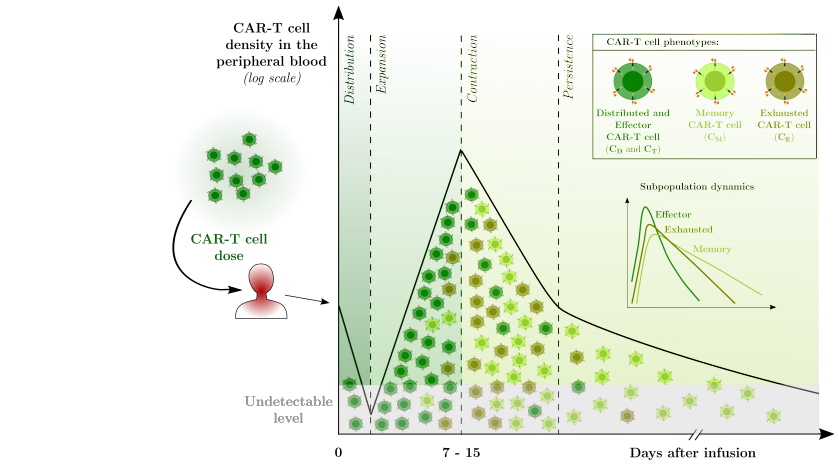

(a)

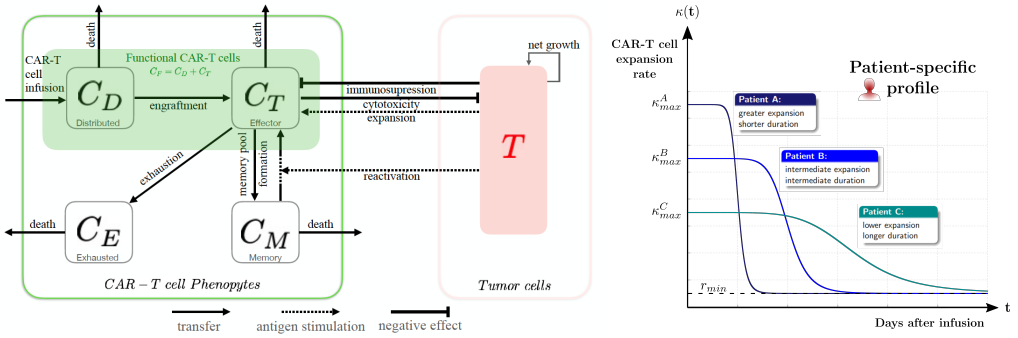

(b) (c)

Figure 1. Multiphasic CAR-T cell dynamics. (a) Schematic representation of the multiphasic response to CAR-T cell therapy as described by the model. After CAR-T infusion, the typical response profile shows a rapid and usually undetectable decline of circulating CAR-T cells, featuring the distribution phase. The expansion phase is characterized by the antigen-mediated proliferation of engrafted CAR-T cells and reaches its peak about two weeks after starting treatment. Over time, effector cells contribute to the formation of the memory cells but also loose proliferative and cytotoxic capacities, becoming exhausted CAR-T cells. The expansion peak is followed by a contraction phase, marked by a sharp decay of CAR-T cells. The longer lifespan of memory cells leads to a long period of smooth decline, which characterizes the persistence phase. (b) Schematic description of the CAR-T immunotherapy model in patients. The CAR-T cells infused into the patient undergo a rapid distribution phase (C_D). A part of these cells undergoes engraftment and establish themselves in the blood and tumor niche. Engrafted cells are called effector CAR-T cells (C_T) and expand upon antigen contact, differentiate into memory CAR-T cells (C_M), become exhausted (C_E), and die naturally or are targeted by tumor immunosuppressive mechanisms. Both C_T and C_D populations present cytotoxic effect and, therefore, are named functional CAR-T cells. Memory CAR-T cells die naturally but are readily responsive to antigen-positive cells. When they interact with tumor cells, they differentiate back into effector CAR-T cells, producing a rapid immune response against the tumor. Over time, effector CAR-T cells become exhausted and are eliminated. Tumor cells (T), which express the specific target antigen, grow depending on the resources available in the microenvironment and are killed by functional CAR-T cells. The net growth of tumor cells results from the balance between their proliferation and natural death. (c) Illustrative patient profiles of the function $\kappa(t)$, describing the antigen-mediated and time-dependent expansion rate of engrafted CAR-T cells. Individual characteristics and heterogeneity of the infused product ultimately define the strength and duration of each phase of the CAR-T cell dynamics.

Preprints (www.preprints.org) | NOT PEER-REVIEWED | Posted: 23 September 2022 doi:10.20944/preprints202209.0359.v1

The CAR-T cell population is divided into three phenotypes: functional, memory, and exhausted CAR-T cells. The functional CAR-T cells are activated T lymphocytes that present cytotoxic effect. They are further split into two compartments, distributed and effector cells. This allows the description of the following biological characteristics: (i) circulating CAR-T cells in PB may be detectable only a few days after infusion during which CAR-T cells are distributed in the patient's body (Lee *et al.* [3] reported that median values of absolute circulating CAR-T cells are detectable only 5 to 9 days after injection, although the median values of tumor cells in PB have already been reduced by this time); (ii) the duration of the distribution phase depends on the disease (it is very fast in ALLs, being undetectable by blood tests, while it is well marked in DLBCLs [22]); (iii) most of the cells that are infused into the patient do not undergo engraftment (only dozens to hundreds of CAR-T clones give rise to the future *in vivo* oligoclonal population of CAR-T cells [29]; there are patients for whom it has been reported that only a single clone can be responsible for response and persistence [30,31]).

2.1. Mathematical model

Our model describes the dynamics of an immunotherapeutic treatment with CAR-T cells in patients with hematological cancer. Non-functional CAR-T cells and untranslated T lymphocytes would not engraft and thus, they were not considered in the model. Let C_D denote the number of distributed CAR-T cells and C_T the number of engrafted CAR-T cells that circulate in the PB and in the tumor niche. These functional CAR-T cells are denoted by $C_F = C_D + C_T$, and consist of CAR-T cells that have cytotoxic activity, quickly recognize specific antigen expressed by the tumor cells, and are ready to target them. Engrafted CAR-T cells may differentiate into memory cells, denoted by C_M, or become exhausted cells, denoted by C_E. Our mathematical model for the response of CAR-T cell immunotherapy against B-cell malignancies, denoted by T, in patients is given by

$$\frac{dC_D}{dt} = -(\beta + \eta)C_D\,, \tag{1a}$$

$$\frac{dC_T}{dt} = \eta C_D + \kappa(t)F(T)C_T - (\xi + \epsilon + \lambda)C_T + \theta T C_M - \alpha T C_T\,, \tag{1b}$$

$$\frac{dC_M}{dt} = \epsilon C_T - \theta T C_M - \mu C_M\,, \tag{1c}$$

$$\frac{dC_E}{dt} = \lambda C_T - \delta C_E\,, \tag{1d}$$

$$\frac{dT}{dt} = rT(1 - bT) - \gamma f(C_F, T)T\,, \tag{1e}$$

in which the total number of functional CAR-T cells is

$$C_F = C_D + C_T \tag{2}$$

and the functions $\kappa(t)$, $F(T)$, and $f(C_F, T)$ are given by

$$\kappa(t) = r_{min} + \frac{p_1}{1 + (p_2\, t)^{p_3}}, \qquad F(T) = \frac{T}{A + T}, \tag{3}$$

$$f(C_F, T) = \frac{\dfrac{C_F}{T}}{\vartheta + \dfrac{a + C_F}{T}}. \tag{4}$$

An overview of the considered interaction mechanisms is provided in Figure 1b and the biological meaning and units of each parameter are given in Table 1.

The model assumes that, after infusion, CAR-T cells are distributed in the patient's body. Distributed CAR-T cells have a natural death rate β, and an engraftment rate

Preprints (www.preprints.org) | NOT PEER-REVIEWED | Posted: 23 September 2022 doi:10.20944/preprints202209.0359.v1

Table 1: Model parameters with its units and biological meaning.

Parameter	Unit	Biological meaning
β	day^{-1}	Reduction rate of infused cells due to natural death during their distribution in the patient's body
η	day^{-1}	Engraftment rate of injected cells to blood and tumor niche
r_{min}	day^{-1}	Minimum expansion rate of effector CAR-T cells
p_1	day^{-1}	Initial expansion rate of effector CAR-T cells
p_2	day^{-1}	Rate that regulate the duration of maximum expansion period of effector CAR-T cells
p_3	-	Expansion coefficient that regulates the decay of maximum expansion period of effector CAR-T cells
A, a	cell	Half-saturation constants of functions $F(T)$ and $f(C_T, T)$
ξ	day^{-1}	Death rate of effector CAR-T cells
ϵ	day^{-1}	Conversion rate of effector CAR-T cells into memory CAR-T cells
λ	day^{-1}	Exhaustion rate of effector CAR-T cells
θ	$(\text{cell.day})^{-1}$	Conversion coefficient of memory CAR-T cells into effector CAR-T cells due to interaction with tumor cells
α	$(\text{cell.day})^{-1}$	Inhibition coefficient of effector CAR-T cells due to interaction with tumor cells
μ	day^{-1}	Death rate of memory CAR-T cells
δ	day^{-1}	Death rate of exhausted CAR-T cells
r	day^{-1}	Maximum growth rate of tumor cells
b	cell^{-1}	Inverse of the carrying capacity of tumor cells
γ	day^{-1}	Cytotoxic rate of the functional CAR-T cells on tumor cells
ϑ	-	Half-saturation constant of the cytotoxic effect on tumor cells

η. Since the solution of (1a) is $C_D(t) = C_D(0)e^{-(\beta+\eta)t}$, the total number of engrafted CAR-T cells (EC) can be calculated as

$$EC \approx \int_0^\infty \eta C_D(t)dt = \left(\frac{\eta}{\beta+\eta}\right)C_D(0)\,, \tag{5}$$

in which $C_D(0)$ denotes the CAR-T cell dose infused at day 0.

The effector CAR-T cells that engraft correspond to the functional CAR-T cells in the PB and in the tumor niche. These cells undergo clonal expansion upon contact with tumor cells, which express the target antigen, at a time-dependent patient-specific rate $\kappa(t)F(T)$. The function $F(T)$ describes the effector CAR-T cell expansion as a process that only occurs in the antigen presence and is limited by intrinsic cell proliferation capacity. This behavior is modeled by the function $0 \leq \frac{T}{A+T} \leq 1$ in (3). The constant A defines the number of tumor cells at which the expansion is half of its maximum value. Function $\kappa(t)$ modulates the antigen-dependent CAR-T cell expansion. At the time of infusion, CAR-T cells are at their maximum expansion capacity which eventually decays towards a basal level. Such dynamics depends on both patient-specific and product heterogeneity characteristics. The design proposed in (3) is inspired in the time-dependent expansion rate developed in [32] to model the expansion of CAR-T memory cells. Here, the time-dependent expansion rate $\kappa(t)$ of effector CAR-T cells depends on four parameters: r_{min} is the basal (or background) CAR-T cell expansion rate [25], p_1 defines the initial expansion rate, while p_2 and p_3 regulate the duration and the decay of the expansion rate, respectively. In Figure 1c, we exemplify 3 different patterns of patient profiles (patients A, B, and C). In these examples, the patients have the same baseline expansion value (r_{min}), which is not always the case. Upon the presence of antigen, the maximum rate of CAR-T cell expansion is $p_1 + r_{min}$. Such expansion is sustained for a certain period, forming a plateau, after which it eventually decays. The plateau width and the decay rate are regulated by parameters p_2 and p_3. In Figure 1c, patient A displays the highest expansion rate (κ^A_{max}), sustained for a shorter period, followed by a sharp decay. In contrast, patient C has a smaller expansion rate (κ^C_{max}) that lasts a longer period of time and decays more smoothly, implying a much longer expansion than that

Preprints (www.preprints.org) | NOT PEER-REVIEWED | Posted: 23 September 2022 doi:10.20944/preprints202209.0359.v1

shown in patient A. Patient B has an intermediate profile with $\kappa^A_{max} > \kappa^B_{max} > \kappa^C_{max}$. Therefore, the function $\kappa(t)$ allows modeling different behaviors of *in vivo* CAR-T cell expansion, taking into account patient-specific characteristics which ultimately define the strength and duration of each phase in CAR-T cell dynamics.

The effector CAR-T cell population is reduced due to natural death, that occurs at a rate of ξ, and the conversion into memory CAR-T cells, at a rate of ϵ. Over time, effector CAR-T cells lose their proliferative and cytotoxic capacities, becoming exhausted cells at a rate of λ. Note that, once exhausted, these cells die naturally, which is modeled by the term δC_E. Moreover, effector CAR-T cell population also increases due to the conversion of memory CAR-T cells back to the effector phenotype upon antigen presence. This behavior is modeled by the term $\theta T C_M$. In addition, tumor cells inhibit effector CAR-T cells through different mechanisms, which are jointly modeled by the term $\alpha T C_T$. This term can model, for example, the inhibitory effect on T cells due to the expression of the intracellular enzyme indoleamine 2,3-dioxygenase (IDO) by the tumor cells [28,33].

The dynamics of memory CAR-T cells is described by the differentiation from effector CAR-T cells, the return to the effector phenotype upon antigen contact, and the natural death at a rate of μ. We assume that the memory phenotype has a longer lifetime than effector phenotype, so that $\mu < \xi$. Note that the memory CAR-T cell phenotype considered here has no cytotoxic activity. In addition, we consider that the formation of the memory pool occurs mainly during the contraction phase of the CAR-T cells [34].

We assume that tumor cells grow following a logistic law, with a growth rate r and carrying capacity $1/b$. The rate at which functional CAR-T cells kill tumor cells is given by $\gamma f(C_F, T)$. As suggested in [34–36], the saturation function $f(C_F, T)$ (4) expresses the access of each functional CAR-T cell to tumor cells. When $T >> C_F$, the decrease of tumor cells in time depends exclusively on C_F, being equal to $\gamma f(C_F, T)T \approx \gamma\, C_F/d$. Otherwise, if $T << C_F$, then the rate of decrease of T in time is limited to γT. The term ϑT defines the cell number at which the function reaches half of the maximum saturation.

2.2. Experimental data

To assess the model capability to describing real and heterogeneous clinical data, we have selected three data sets from the literature concerning CD19-directed CAR-T cell therapy. Measures of CAR-T cell abundance in PB over time are available for individual patients in [22,37,38]. The first data set refers to pediatric and adult with B-ALL, CLL, and DLBCL patients [22]. All patients were treated with autologous second generation CAR-T construct with 4-1BB (CD137) co-stimulatory domain. Data below detection threshold were not used for model calibration. For ALL patients, the dataset does not provide information on the administered dose; for these cases, we adopted a value of 1.0×10^8 cells, corresponding to the median dose of CAR-positive viable T cells for patients weighing > 50 kg and indicated in tisagenlecleucel package insert approved by FDA [21]. For this dataset [22], patient outcomes were not considered in the simulation because they were not reported for all patients. We also analyzed data from [38], which consist of CLL patients treated with cells of autologous origin and costimulatory signal provided by the 4-1BB domain. Detection threshold was 25 copies/μg DNA corresponding to 2.5×10^6 CAR-T cells. CAR-T cells were administrated with a 3-day split-dose regimen (10%, 30%, and 60%), with the total dose reported for each patient. The last selected dataset was obtained from [37] using the software WebPlotDigitizer [39]. This study covered ALL, CLL, DLBCL, and MCL patients, all of them treated with CAR-T cells with CD28 costimulatory domain and were allogeneic (the T cells were obtained from each recipient's alloHSCT donor). As the quantification threshold was not informed in [37], we assumed the same value used in [38], since both used quantitative polymerase chain reaction (qPCR) and reported the outcomes of all patients. Individual dose was informed per kg, and we consider that each patient weighed 60 kg. Information on data transformation is detailed in the Supplementary Material (Section SM-1) together with

Preprints (www.preprints.org) | NOT PEER-REVIEWED | Posted: 23 September 2022 doi:10.20944/preprints202209.0359.v1

the table with the extracted data (Table SM-1). The labels used here to identify patients are the same as defined in the original references.

In [37] and [38], patient outcomes at the last recorded follow-up were available and model parameters were adjusted accordingly. As in [40,41], we considered that patients with complete response (CR) have clinically undetectable tumor burden (below the detection threshold of 2.5×10^6 cells), while partial response (PR) characterizes patients with tumor burden above the detection threshold but below 50% of the initial tumor burden (i.e., 5.0×10^6 cells), and stable disease (SD) indicates patients with tumor burden in the range between $\pm$ 50% of the initial tumor burden (i.e., 5.0×10^6 cells $< T < 1.5 \times 10^7$ cells). For completeness, patients with tumor burden greater than 50% of the initial tumor burden ($T > 1.5 \times 10^7$ cells) are classified as progressive disease (PD), although no PD patient was analyzed in this work.

2.3. Mechanisms underlying the multiphasic dynamics of CAR-T cell therapy

The previously published patient data used here consist of CAR-T cell time courses after injection for different malignancies. It is well know that the dynamical clinical response to CAR-T cell therapy is usually characterized by the following phases: distribution, expansion, contraction, and persistence.

The biological mechanisms underlying this multiphasic response of CAR-T cell therapy can be explained through the analysis of the different time scales occurring in the model dynamics. We first note that the observed clinical data consists of measurements of CAR-T cell counts in the PB or BM samples of patient time courses and does not capture the changes in the composition of the CAR-T population by the different phenotypes. Therefore, we track the behavior of the total CAR-T cell population, which is given by $C = C_D + C_T + C_M + C_E$. The total CAR-T cell dynamics is, therefore,

$$\frac{dC}{dt} = -\beta C_D + \left(\frac{\kappa(t)T}{A+T} - \xi - \alpha T\right)C_T - \mu C_M - \delta C_E \,.$$

We also refer to the *per capita* rate of change in the total CAR-T cell population, given by

$$\frac{1}{C}\frac{dC}{dt} = -\beta\frac{C_D}{C} + \left(\frac{\kappa(t)T}{A+T} - \xi - \alpha T\right)\frac{C_T}{C} - \mu\frac{C_M}{C} - \delta\frac{C_E}{C} \,.$$

Such expressions, together with considerations about the variation on the composition of the CAR-T cell population, reveals the dominant process at each phase. This systematic analysis allows to estimate the model parameters for each patient, as follows. As indicated in the time course data of a general patient depicted in Figure 2a, it is possible to split the dynamics into four well-marked phases, approximated as lines in the logplot of the CAR-T cell population along time, and which can be fitted to the data. The slope of each line (m_d, m_e, m_c, and m_p) can be connected to the corresponding dominant process for modeling the overall patient dynamics. Likewise, the *per capita* population rate of CAR-T cells also helps assessing whether the slopes agree with the variation presented in each phase of the dynamics (Figure 2b).

Distribution phase: at the injection time, the entire CAR-T cell population consists of injected cytotoxic cells that target the tumor cells and may die or engraft. Therefore, at the first phase, the other CAR-T cell populations do not contribute to the model dynamics. Mathematically, we approximate $C_T, C_M, C_E \approx 0$ and $C \approx C_D$. Together with the observation that $\eta << \beta$, we obtain that the change in the CAR-T cell population is approximated by

$$\frac{dC}{dt} \approx -\beta C_D, \quad \text{and} \quad \frac{1}{C}\frac{dC}{dt} \approx -\beta \,.$$

This shows that the initial decline observed in the CAR-T cell population is due to the loss of injected CAR-T cells that do not engraft. Thus, the decline in the clinical data leads to $m_d \approx -\beta$, which provides a first approximation for the parameter β. Figure 2b

Preprints (www.preprints.org) | NOT PEER-REVIEWED | Posted: 23 September 2022 doi:10.20944/preprints202209.0359.v1

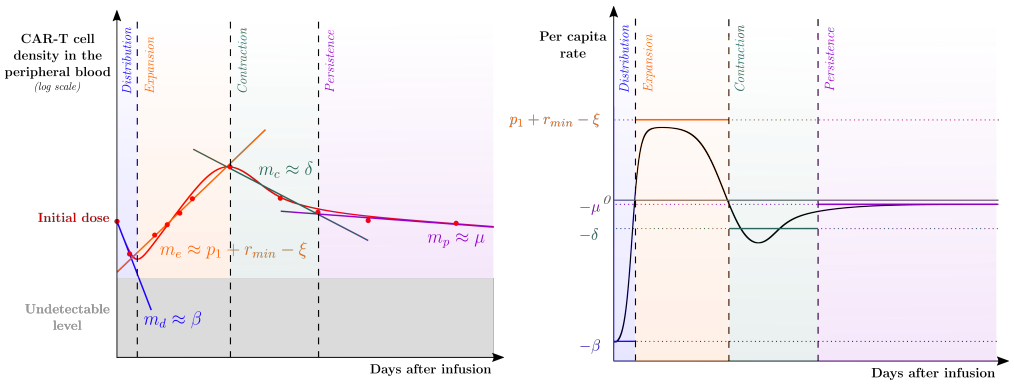

Figure 2. Schematic description of the strategy used to assess the dominant mechanisms underlying the multiphasic CAR-T cell dynamics. (a) Experimental data (●) of CAR-T cell kinetics from a representative patient profile were split among the four phases of CAR-T cell dynamics to which lines in the logplot of the CAR-T cell population along time were fitted. The corresponding (growth or decline) rates are denoted by m_d, m_e, m_c, and m_p, associated with the distribution, expansion, contraction, and persistence phases, respectively. These rates are used as first approximations to the parameters of the leading mechanism(s) of each phase. Specifically, the distribution phase is mainly driven by the reduction rate of the injected CAR-T cells so that $m_d \approx \beta$; the expansion phase is driven by the combined effect between the C_T expansion ($p_1 + r_{min}$) and mortality (ξ), leading to $m_e \approx p_1 + r_{min} - \xi$; the contraction and persistence phases are mainly driven by the mortality of exhausted and memory CAR-T cells, respectively, which yield $m_c \approx \delta$ and $m_p \approx \mu$. (b) The *per capita* rate of the total CAR-T cell population ($C_D + C_T + C_E + C_M$) is displayed over time after infusion together with the calibrated values of β, $p_1 + r_{min} - \xi$, δ, and μ.

shows that m_d has indeed provide a good approximation for the initial *per capita* rate of the total CAR-T cell population.

Expansion phase: the second phase is characterized by an exponential growth of the CAR-T cell population. Assuming that the injected cells already died or engrafted, and that there was not enough time for a substantial part of the engrafted effector population to become exhausted neither transit to a memory phenotype, we have that $C_D, C_M, C_E \approx 0$ and $C \approx C_T$. Let us further assume that the tumor load presents values that still stimulate the CAR-T expansion, i.e., $T/(A+T) \approx 1$, and that the tumor immunosuppressive effects are negligible ($\alpha T \approx 0$). Finally, assuming that the initial expansion level of the effector CAR-T cells has not decreased to its basal level, we have $\kappa(t) \approx r_{\min} + p_1$. With these assumptions, the dynamics of the CAR-T cell population is approximated by

$$\frac{dC}{dt} \approx (r_{\min} + p_1 - \xi)C_T, \quad \text{and} \quad \frac{1}{C}\frac{dC}{dt} \approx r_{\min} + p_1 - \xi\,.$$

This indicates that the CAR-T cell expansion observed in the second phase results from the net effect of combining the initial expansion of effector CAR-T cells (p_1), their basal expansion rate ($r_{\min}$), and their natural mortality (ξ). This leads to $m_e \approx r_{\min} + p_1 - \xi$, allowing a first approximation to the values of the parameters $r_{\min}$, p_1, and ξ. At the end of the calibration process, Figure 2b shows that m_e is slightly larger than the *per capita* rate of CAR-T cells during the expansion phase, probably due to the formation of memory and exhausted CAR-T cells.

Contraction phase: the third phase is characterized by an steep decline of the CAR-T cell population. During this phase, the expansion rate of effector CAR-T cells reduced to its basal level ($\kappa(t) \approx r_{\min}$) and the intense decrease of the tumor burden reduced

Preprints (www.preprints.org) | NOT PEER-REVIEWED | Posted: 23 September 2022 doi:10.20944/preprints202209.0359.v1

the antigen availability so that $\kappa(t)T/(A+T) \approx 0$. Therefore, the mortality process dominates the dynamics, yielding

$$\frac{dC}{dt} \approx -\xi C_T - \mu C_M - \delta C_E \, .$$

Assuming that the memory CAR-T cells have the lowest death rate and that the memory population is smaller than the others, we have $\mu C_M << \xi C_T + \delta C_E$. Thus, the dominant process is the mortality of effector and exhausted CAR-T cells. Further, the exhaustion of the remaining effector cells leads to a higher number of exhausted cells in comparison with effector cells. Therefore, $\xi C_T << \delta C_E$. Thus, the strong contraction of the CAR-T cell population after the peak is dominated by the elimination of effector and, mainly, exhausted CAR-T cells:

$$\frac{dC}{dt} \approx -\xi C_T - \delta C_E \approx -\delta C_E, \text{ and } \frac{1}{C}\frac{dC}{dt} \approx -\delta \, .$$

This allows to identify the m_c observed in the clinical data with the mortality rate of exhausted CAR-T cells, $m_c \approx -\delta$. When comparing such an approximation with that depicted in Figure 2b, observed differences may be owed to the mortality of the other population phenotypes.

Persistence phase: finally, the fourth phase is characterized by a slower decline in the CAR-T cell population. Taking into account the previous phases, we may assume that the CAR-T cell population is comprised of almost only memory cells. Therefore, we have

$$\frac{dC}{dt} \approx -\mu C_M \text{ and } \frac{1}{C}\frac{dC}{dt} \approx -\mu \, .$$

Thus, the slope m_p observed in the clinical data resembles the mortality rate of memory CAR-T cells, $m_p \approx -\mu$. As shown in Figure 2b, m_p actually provides a good approximation for the *per capita* rate of the total CAR-T cell population in the persistence phase.

The present analysis shows that the behavior of each phase is influenced by the specific biological characteristics of the most abundant phenotype. The C_D, C_T, C_E, and C_M phenotypes are determinants for the distribution, expansion, contraction, and persistence phases of the *in vivo* CAR-T cell kinetics, respectively. The identification of the dominant mechanisms underling each CAR-T cell phase drives the model calibration procedure for each patient-specific scenario, as presented in the Supplementary Material (Section SM-2). Such initial approximations may be over or under estimations depending on the validity of the corresponding assumptions in the individual scenario, which is assessed after the calibration procedure.

2.4. Model Settings and Numerical Solution

Model equations (1) were solved numerically using the explicit fourth-order Runge–Kutta method [42], with $\Delta t = 10^{-4}$ days. The initial tumor burden, not reported for most of the analyzed patients, was always set as $T(0) = 10^7$ cells. The infused dose of CAR-T cells is the initial condition of the distributed CAR-T cell population ($C_D(0)$). The initial populations of the other phenotypes are assigned to zero since the phenotypic differentiations occur throughout the evolution of the dynamics.

The model was adjusted for each individual patient, considering the corresponding reported data and response to therapy, when available. Some of the model parameters (r, b, γ, and ϑ) were fixed with values from the literature [26], although the value of γ was also changed for some patients. Extensive tests were carried out to obtain the complete (non-unique) set of parameter values for each patient, whose initial approximations were obtained from the analysis presented in Section 22.3, as described in the Supplementary Material (Section SM-2). All sets of calibrated parameters are shown in Tables SM-2, SM-3, and SM-5.

Preprints (www.preprints.org) | NOT PEER-REVIEWED | Posted: 23 September 2022 doi:10.20944/preprints202209.0359.v1

3. Results

The proposed model (1) is used to describe the multiphasic kinetics of the total CAR-T population for different hematologic cancer types and therapy responses. The CAR-T cell population encompasses functional (distributed and effector), memory, and exhausted CAR-T phenotypes, whose interactions improve the understanding of the key factors that influence the dose-exposure-response relationship. Model calibration was performed for each patient-specific data using the multi-step strategy based on the mechanisms underlying the multiphasic dynamics of the CAR-T cell therapy (see Section SM-2). Good agreement with the data was then obtained using such strategy, as shown in Figure SM-1. The relation between the area under the curve of total CAR-T cells and the corresponding fraction of non-exhausted phenotypes provided a significant characterization of patient responses.

3.1. Description of the cellular dynamics of CAR-T therapy applied to different hematological cancers

We first present the results of fitting the model to the data obtained from Liu *et al.* [22]. A total of 12 patients were selected and grouped according to the type of cancer: DLBCL, pediatric and adult ALL, and CLL. All patients received a single dose of CAR-T cells on day zero. Patient-specific model simulations of CAR-T cell dynamics are shown in Figure 3, as well as the corresponding time-dependent CAR-T expansion rates ($\kappa(t)$). In the Supplementary Material, we show model simulations on linear scale of total CAR-T cells and tumor burden in Figure SM-2 and the measures of fit quality in Figure SM-6.

Figure 3 shows that our model was able to capture the diversity of behavior of the dynamics of CAR-T cells in different types of cancer and patients. We note that the distribution phase is well marked for patients with DLBCL, as already reported in [22]. Regardless of the duration of the distribution phase, similar goodness of fit is observed for all patients, even in those in which it lasts less, as in ALL pediatric patients (see Figure SM-6). The total number of engrafted CAR-T cells showed great variation between patients, ranging from 2 to 5-fold magnitude orders lower than the initial dose. Patient L (pediatric ALL) recorded the highest engraftment with EC equal to approximately the infused total CAR-T cell dose (see Table SM-2). The expansion phase was also well characterized with CAR-T peak values reached between one and two weeks after initial dose for most patients. Likewise, the model was also able to represent the dynamics of patient UPN10 whose expansion peak occurred late on day 54. The time of maximum concentration of total CAR-T cells matches the peak of the effector phenotype and marks the beginning of the contraction phase. The exhausted and memory CAR-T cells, which are formed and mostly grow during the expansion phase, peak shortly after the start of the contracion phase. Meanwhile, effector CAR-T cells undergo a sharp decrease and are eventually replaced by exhausted CAR-T cells. The decrease of exhausted CAR-T cells due to natural death eventually leads the CAR-T cell population to be mostly formed by long-lasting memory CAR-T cells, starting the persistence phase.

The patient-specific expansion profiles described by function $\kappa(t)$ directly reflect the characteristics of the CAR-T cell dynamics, as shown on the bottom row of Figure 3. Patients with later CAR-T cell peaks have more evident plateaus in their $\kappa(t)$ functions, whereas there are no plateaus for patients depicting earlier CAR-T cell peaks. Consider, for example the DLBCL patients. They all have different maximum expansion and decay rates, but the same minimum expansion rate. Their expansion profiles are different: they all exhibit plateaus but with different widths and decays to the minimum value. Patient 30 presented the highest expansion and the latest peak; patient 28 showed less expansion and earlier peak; and patient 27 exhibited the much slower expansion rate decay. However, the therapy performed on patient 28 was able to eliminate the tumor faster and the effector phenotype persisted longer due to the lower natural mortality

 doi:10.20944/preprints202209.0359.v1

rate. Pediatric ALL patients, on the other hand, do not have maximal expansion plateaus like those with DLBCL, and the dynamics starts with the maximum rate of CAR-T cell expansion which soon decays.

Overall, the CAR-T cell dynamics of the patients analyzed in this section were well represented by the proposed model. The analysis did not take into account the corresponding therapy responses since they were not available for all patients. Nevertheless, it was possible to associate the dynamics of the different phenotypes of CAR-T cells with the observed interindividual variability among the selected patients. In the next section, we analyze a new dataset that integrates the therapy outcomes.

3.2. Description of the cellular dynamics of CAR-T therapy applied to patients with different outcomes

We next analyze the two datasets obtained from [37,38]. To distinguish them, we added the letters B or P before the original identifications of patients selected from Brudno *et al.* [37] and Porter *et al.* [38], respectively. Patients from [37] received a single dose of CAR-T cells while fractionated doses (10%, 40%, and 60%) were infused at days 0, 1, and 2 in patients from [38]. The 12 selected patients were then grouped as CR (complete response), PR (partial response), or SD (stable disease) according to their responses to therapy as assessed by the tumor burden at the last follow-up data. Patient-specific model simulations of CAR-T cell dynamics are shown in Figure 4, as well as the corresponding time-dependent CAR-T expansion rates ($\kappa(t)$). In the Supplementary Material, we show model simulations on linear scale of total CAR-T cells and tumor burden in Figure SM-3 and the goodness of fit is also plotted in Figure SM-6.

Patients from [37] have less cellular kinetic data than those reported in [38]. For patient B10, for example, there are no data points in the contraction and/or persistence phases. In cases like this, a good characterization of the behavior of these phases is not possible. Model calibrations in these scenarios were then made in order to fit to the therapy responses. Figure 4 (and Figures SM-3 and SM-6) shows that the proposed model was able to represent well the diversity of behaviors and responses of the analyzed patients. The total number of engrafted CAR-T cells also showed large variation, ranging from the engraftment of approximately the full dose (Patient P22-PR) to just a single cell (Patients B5-CR and B11-PR). The other patients recorded ECs ranging from the same order of magnitude of the infused CAR-T cell dose to eight orders of magnitude smaller (see Table SM-3). The expansion profile of each patient, shown on the bottom row of Figure 4, also reflects the dynamics well: longer and higher plateaus correlate with later peaks and with higher CAR-T cell concentrations, although the absolute value of the peak depends on other factors. For example, CAR-T cell peaks reached by patients B15-CR and P1-CR are similar while κ_{max}^{P1} is more than four times greater than κ_{max}^{B15}. Interestingly, some other interindividual variabilities emerge from the present analysis, as we show in what follows.

Patient P12 exhibits a peak with greater abundance of exhausted cells. The population of effector CAR-T cells lasts around 3 weeks due to a sharp decline during the contraction phase. However, there was enough time to form a memory pool which outnumbers the population of exhausted CAR-T cells for a short period of time. After 72 days, effector CAR-T cells resume growth but at undetectable levels. The memory-effector cell conversion is due to the antigen expressed by cancer cells which grow at undetectable for 6 months, when they reach the detection threshold. The CAR-T cell dynamics for Patient P22 was characterized by a very short distribution phase, higher peak concentration than in patient P12, which allowed greater memory formation. This, combined with a smaller amount of exhausted cells, delayed the tumor's relapse, which occurred in 300 days. CAR-T cell persistence with loss of cytotoxic function has already been reported in [6].

Preprints (www.preprints.org) | NOT PEER-REVIEWED | Posted: 23 September 2022 doi:10.20944/preprints202209.0359.v1

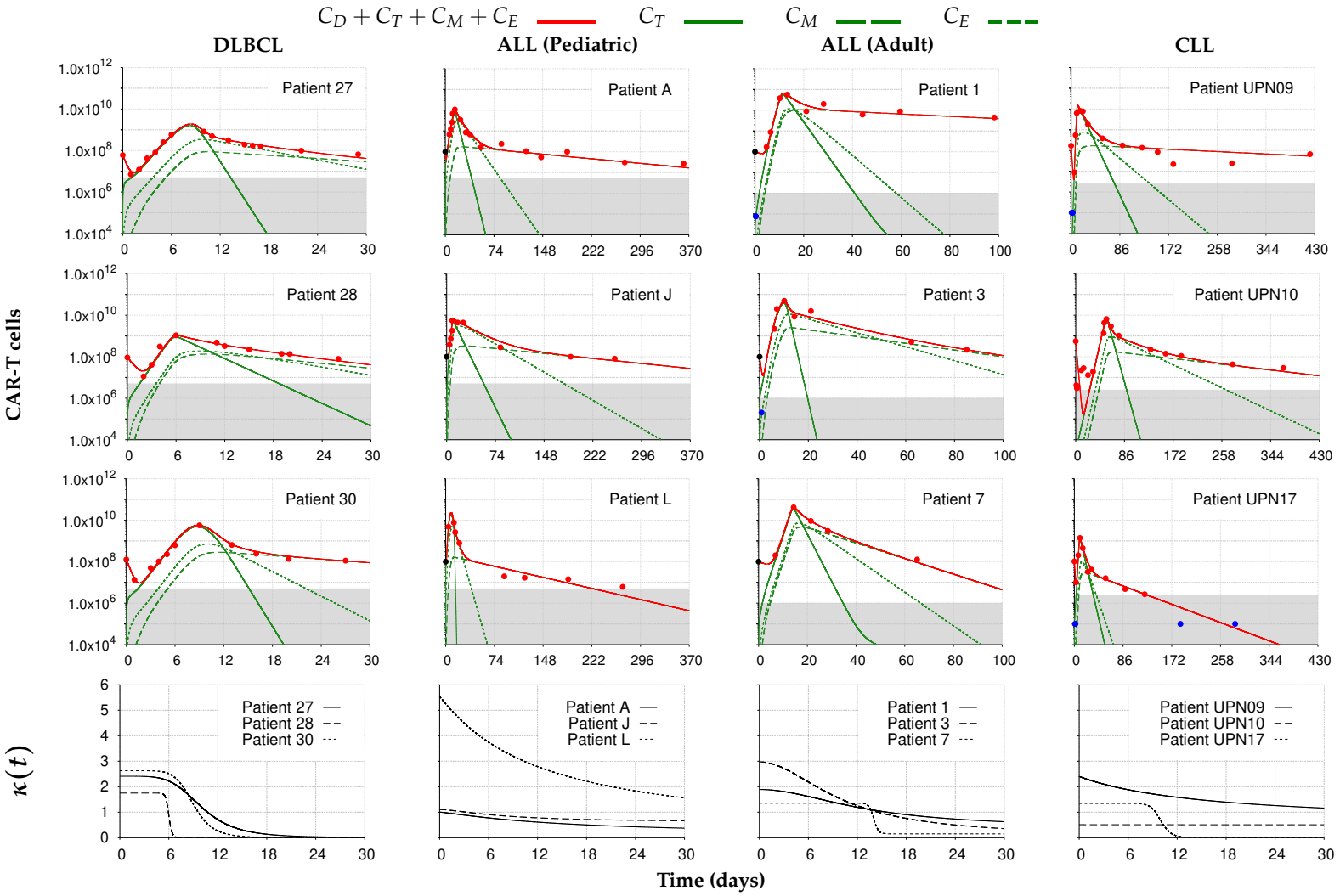

Figure 3. Model simulations fitted to the experimental data (●) from [22]. Each column corresponds to the dynamics of the total CAR-T cell population (—) for different diseases (DLBCL, pediatric and adult ALL, and CLL) and different patients. The total CAR-T cell population is divided into CAR-T effector (C_T), memory (C_M), and exhausted (C_E) phenotypes, shown in continuous, dashed, and dotted green, respectively. The mean dose value of 1.0×10^8 cells (●) presented in [21] is used as a surrogate for the actual doses when not reported for patients with ALL. The gray region represents the undetectable levels (below the threshold of 5.0×10^6 cells to DLBCL and pediatric ALL, 1.0×10^6 cells to adult ALL, and 2.5×10^6 cells to CLL [22]). Data points in this region (●) were not used for calibration and error calculation due to their high uncertainties. The bottom row presents the time-dependent expansion rate function ($\kappa(t)$) for each patient.

 doi:10.20944/preprints202209.0359.v1

Patients who reached SD exhibited good expansion profiles with CAR-T cell peaks formed predominantly by effector cells but with significant exhaustion and undetectable levels of memory. Patients B2 and B10 did not present detectable persistence phase. However patient B18 presented this phase mostly formed by exhausted phenotype.

Among patients in the CR group, all depicted good expansion profiles, with CAR-T cells peaking around day 7 or earlier, except for patients B5 and P2, whose peaks occurred on days 10 and 25, respectively. Patient B12 was the only that did not exhibit detectable persistence phase, although his/her tumor burden remained undetectable in 480 days. Patients P1 and P2 have been followed for a long time after therapy. Their expansion rate functions are remarkably different: $\kappa(t)$ has a narrow initial plateau followed by an abrupt decrease to a relatively high level of basal growth for P1, while the maximum expansion rate of P2 is kept close to the basal level. These properties correlate with the highest expansion and earlier peak for P1 and with the lowest expansion and late peak for P2. With the identification of the distribution and expansion phases of these two patients, it was possible to observe their different engraftment capabilities measured by EC: it was ≈ 12 cells for patient P1 while P2 reached a much higher value of $\approx 10^5$ cells (see Table SM-3). Recently, Melenhorst *et al.* [5] published the 10-year follow-up of these two patients who have remained tumor-free (CR). We have then extended our model simulations up to 3600 days for these two patients to compare with the long-term additional data provided in [5] (the additional data are shown in Table SM-4). Figures SM-4(a) and SM-4(c) show the corresponding model predictions that match clinical outcomes, with undetectable tumor burdens up to 10 years. We have also performed a new model calibration for patient P2, taking into account the complete dataset. Parameter values are shown in Table SM-5 and the model simulation is shown in Figure SM-5(b). The main difference between the two simulations for patient P2 is that the persistence phase is shown to last much longer when integrating the additional data from [5].

3.3. Assessment of patient outcomes through kinetic parameters

We next perform additional analyses of the presented simulations in Figure 4 by evaluating other parameters that could be correlated with therapy responses. A typical parameter is the area under the concentration-time curve (AUC), which is calculated here for the fractions of CAR-T cell phenotypes. We computed AUC from day 0 to day 28 (AUC0-28) because therapy response is usually assessed on day 28, but we also evaluated AUC from day 0 to both day 60 (AUC0-60) and day 90 (AUC0-90) to identify whether CAR-T cell dynamics at later times may also play significant role on the treatment response. The top panel of Figure 5 shows the AUC pie charts for each patient, indicated in each column. The pie radius represents the absolute values of the area. Comparing the areas calculated up to 28, 60, and 90 days, we notice that the pattern of the contribution of each phenotype in the AUC is already defined in the first 28 days of the dynamics in most patients, accompanied by an increase in the amount of the memory phenotype over time. The CAR-T kinetics of CR patients are characterized by higher fractions of memory phenotype in the AUCs than in SD and PR patients, except in P22. This is probably due to the fact that P22 has undergone Richter transformation and got DLBCL arising from CLL with CD19-dim cells at 180 days after infusion [38]. Among PR patients, P12 has the highest AUCs although with a majority fraction of exhausted cells. SD patients have the lowest AUC values, with significant fractions of exhausted cells and less than 0.01% of memory cells.

The middle panel of Figure 5 shows bar plots, for each patient, of the total amount of CAR-T cells at the time of the peak (t_{peak}), denoted by $C(t_{peak})$, with the indication of the amounts of each phenotype, and the ratio between $C(t_{peak})$ and the therapeutic dose ($C(t_{peak})/dose$), which provides the number of times that CAR-T cells expanded with respect to the total infused dose. This ratio may be useful since there are patients with lower doses who exhibit high expansions and the other way around. The results

 doi:10.20944/preprints202209.0359.v1

in Figure 5 show that there is no clear relation between these two parameters and the therapy response. Patients B20 and P2 have quite different expansion profiles but both reached CR; all SD patients display higher $C(t_{peak})/dose$ than patient P1; patient B11 displays an expansion ratio similar to B20, but their AUCs differ in both the absolute values and the fraction of memory cells. For all patients, the CAR-T cells at the peak are made up mostly of functional cells.

Finally, the bottom panel of Figure 5 shows the theoretical (predicted) relapse time (t_{TR}) and the number of CAR-T cells at that time ($C(t_{TR})$), with the corresponding amounts of each phenotype. For most patients, the amount of CAR-T cells at the time of relapse is very small and below the detection threshold. Patients P12, P22, and B18 exhibited the highest $C(t_{TR})$ values but with practically only exhausted cells. We have extended the time of simulations for the decade-long patients P1 and P2 up to 20,000 days. Our predictions indicate a slight small increase in their tumor burdens at non-detectable levels and so no theoretical relapse. For completeness, the values used in the construction of Figure 5 are presented in Table SM-6.

The previous results have shown that a single parameter was not able to correlate to the therapy response. Regarding AUC0-28, for example, low values were obtained for both CR patients (B15, B12 and P2) and SD patients. Considering only the formation of the memory pool, patient B12, who reached CR, formed fewer memory cells than PR patient P12. Moreover, patients P1-CR and B18-SD have similar profiles of functional CAR-T cells. In an attempt to identify whether any combination of parameters could provide insights into the long-term therapy response, we analyzed the parameters considered in Figure 5. Focus was given on the parameters associated with the beginning of the therapy, encompassing AUC0-28, the corresponding fraction of non-exhausted CAR-T cells ($C_D + C_T + C_M$), and quantities $C(t_{peak})$, t_{peak}, and $C(t_{peak})/\text{dose}$. The plots with some combinations of two of these parameters at a time for all patient outcomes are shown in Figure 6. The plot between AUC0-28 and the fraction of non-exhausted CAR-T cells, depicted in Figure 6a, yields the best separation among the response groups. All SD patients display low exposure to CAR-T cells (AUC0-28 $< 5.0 \times 10^{10}$ cell·day) with fractions of non-exhausted cells below 0.8. CR patients have high fractions of non-exhausted CAR-T cells, although their AUC0-28 values vary greatly. PR patients are characterized by intermediate values of AUC0-28. Patient P12 displays the highest production of exhausted cells while patients P22 and B11 produced the lowest. However, it is noteworthy that P22 (marked with △) had undergone a CD19 negative relapse and there is no information on the cause of patient B11 relapse. The separation among the CR, PR, and SD groups, although without clear delimitation, is also observed using the areas up to days 60 and 90. This suggests that the joint assessment of AUC0-28 and the corresponding fraction of non-exhausted CAR-T cells plays important role on patient-specific long-term outcomes. Other parameter combinations do not provide similar separation among the response groups as illustrated in Figures 6b and 6c, which show the plots combining AUC0-28 with $C(t_{peak})$ and $C(t_{peak})/\text{dose}$ with the fraction of non-exhausted CAR-T cells up to 28 days, respectively. Overall, although the joint assessment of AUC0-28 and the fraction of non-exhausted CAR-T cells seems promising, the present analysis is limited to the small number of patients and must be revised by integrating a larger patient cohort.

Preprints (www.preprints.org) | NOT PEER-REVIEWED | Posted: 23 September 2022 doi:10.20944/preprints202209.0359.v1

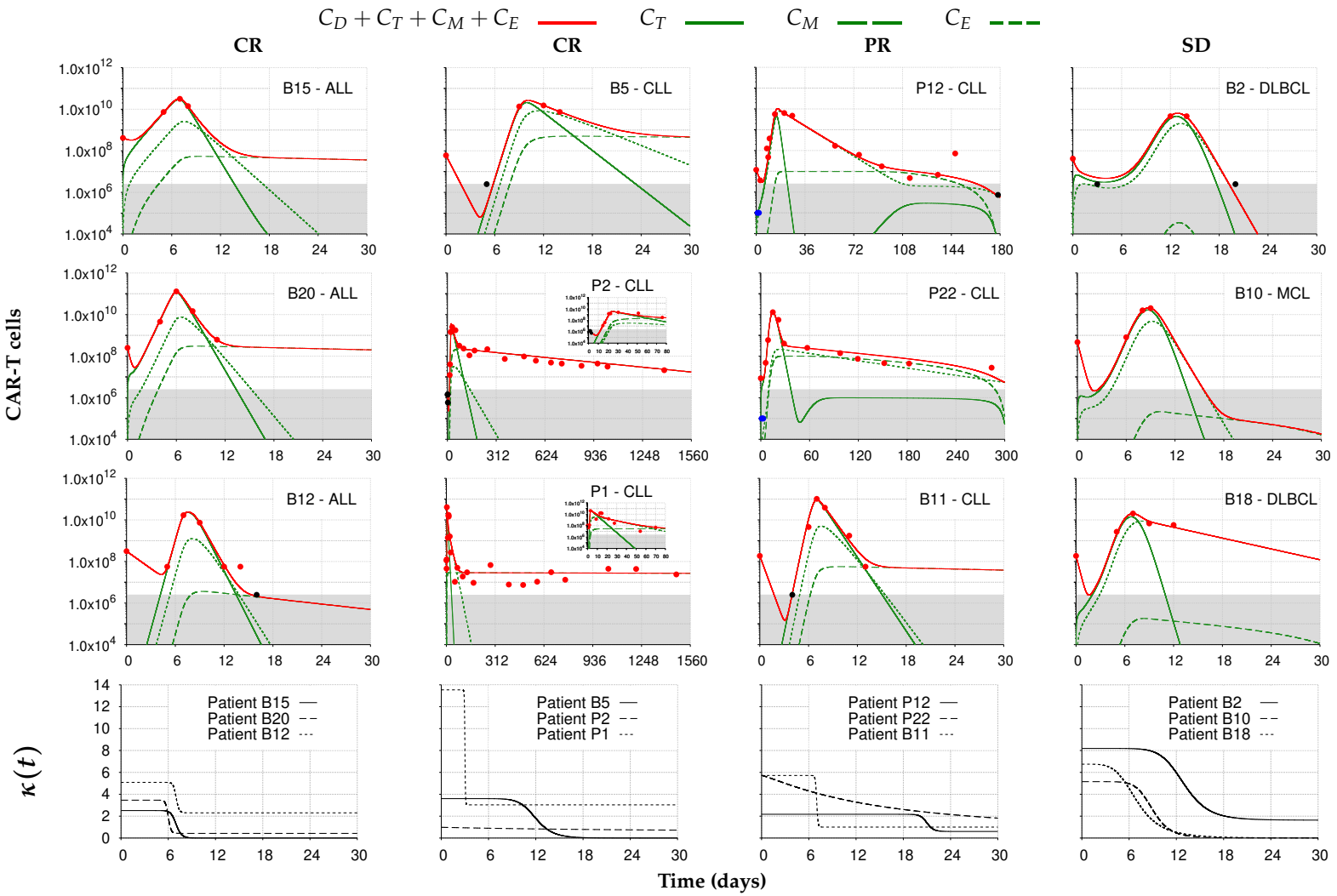

Figure 4. Model simulations fitted to the experimental data (●) from [37,38]. Each column corresponds to the dynamics of the total CAR-T cell population (—) for different therapy responses at last follow-up (interval from infusion to last follow-up in days) (CR – complete response; PR – partial response; SD – stable disease) and different patients. The total CAR-T cell population is divided into CAR-T effector (C_T), memory (C_M), and exhausted (C_E) phenotypes, shown in continuous, dashed, and dotted green, respectively. The gray region represents the undetectable level. Data points (●) may assume any value in this region, but some (●) was not used for calibration and error calculation of the model due to their greater uncertainty. The bottom row presents the time-dependent expansion rate function ($\kappa(t)$) for each patient.

Preprints (www.preprints.org) | NOT PEER-REVIEWED | Posted: 23 September 2022 doi:10.20944/preprints202209.0359.v1

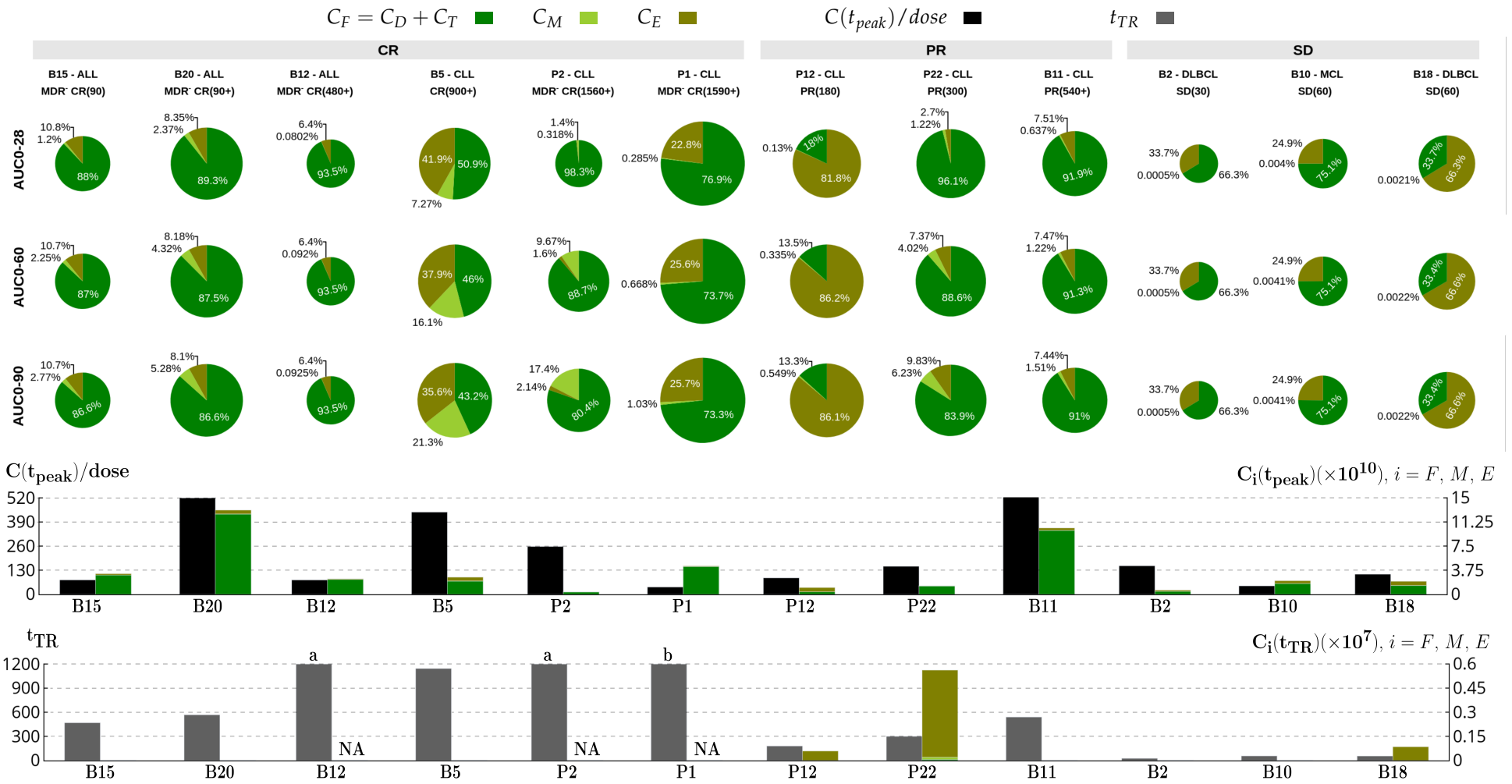

Figure 5. CAR-T therapy outcomes for different patients (one in each column) with ALL, CLL, MCL, or DLBCL with different therapy responses (CR – complete response; PR – partial response; SD – stable disease). Pie charts display the fractions of functional, memory, and exhausted cells composing the area under the curve of the entire CAR-T population during the first 28 (first row), 60 (second row), and 90 (third row) after infusion; absolute values of AUC are indicated by the radii of the pies. The bar plot in the fourth row shows the ratio between the CAR-T cell peak value and the infused dose (in black), along with the amount of each CAR-T cell subpopulation (green tones) on the day when subpopulation at the peak time. The bar plot at the bottom presents the time of the theoretical relapse (t_{TR}, gray) and the corresponding CAR-T cell subpopulations (green tones). NA (not applicable) indicates no theoretical relapse due to: (a) occurrence of limit cycle at undetectable level; (b) no tumor recurrence within 20,000 days.

Preprints (www.preprints.org) | NOT PEER-REVIEWED | Posted: 23 September 2022 doi:10.20944/preprints202209.0359.v1

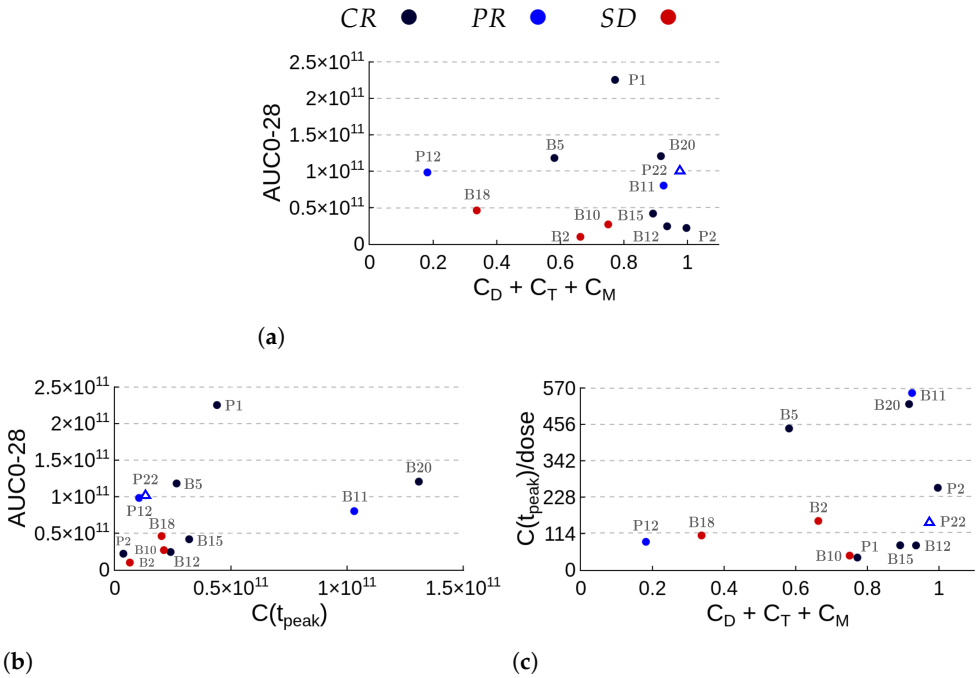

Figure 6. Summary of patient outcomes with respect to kinetic parameters, in appropriate units. Panel (a) highlights the importance of the fraction of non-exhausted cells ($C_D + C_T + C_M$) in the first 28 days after infusion together with AUC0-28. Patient outcomes are concentrated in three distinct regions. Fully responsive patients (CR) have high fractions of non-exhausted cells while patients who achieved stable disease (SD) have small AUC0-28 values with fractions of non-exhausted CAR-T cells below 0.8. Of the three patients who achieved partial response (PR), patient P12 displays moderate value of AUC and a high percentage of exhausted cells. Patients P22 and B11 also have moderate AUC values but small fraction of exhausted cells. Of note, there is no information on the cause of patient B11 relapse but patient P22 (marked with △) underwent mutation with CD19-dim cells. The relationships between AUC0-28 and $C(t_{peak})$ (b), and $C(t_{peak})$/dose and fractions of $C_D + C_T + C_M$ (c) are also considered but do not provide clear separation among the response groups.

4. Discussion

We describe CAR-T cell therapy with a multi-compartment model considering the interactions between tumor cells and different CAR-T cell phenotypes: functional CAR-T cells (encompassing infused cytotoxic CAR-T cells and proliferative engrafted cytotoxic CAR-T cells), memory CAR-T cells, and exhausted CAR-T cells. Previous models successfully described CAR-T cell dynamics in a step-wise approach, i.e., by splitting the time domain into intervals corresponding to the distribution, expansion, contraction, and persistence phases, and considering different sets of differential equations in each time interval [21,22,43]. Through a single set of differential equations based on mechanistic hypothesis, our model reproduces the multiphasic dynamics of CAR-T cells over time for different hematological cancers and therapy responses, providing insights into the role of each of the CAR-T phenotypes along the dynamics. By analyzing the underlying mechanisms that govern each phase, we identify the roles of each CAR-T phenotype in each phase: the distribution phase is due to the loss of injected CAR-T cells that do not engraft; the expansion phase is characterized by increased proliferation of engrafted CAR-T cells; the contraction phase results from a decrease in such proliferation together with exhaustion of effector CAR-T cells; the persistence phase describes the survival and slow decay of memory cells. Besides providing insights into the such mechanisms, this analysis also allows us to develop a systematic approach for patient-specific model calibration based on experimental data, which make this step faster and more accurate.

 doi:10.20944/preprints202209.0359.v1

The division of CAR-T cells into phenotypes and their role in therapy response may also contribute to the identification of possible clinically relevant parameters that correlate with long-term response. Most of the available data on individual patient response to CAR-T therapy consists of time courses of the total CAR-T cell population. In the literature, there are records of the influence of the maximum amount of CAR-T cells and the exposure time on therapy outcomes [3,38,44], although relevant parameter markers have not been well established yet. Huang *et al.* [2] suggested that other factors than dose may help to predict the effectiveness of CAR-T cell therapies due to limited knowledge about dose-response relationships of approved treatments. Also, single evidences on exposure-response relationships may be insufficient to guide clinical development of optimal therapy. The present work sheds light on the importance of understanding the evolution of CAR-T cell phenotypic constitution for investigating CAR-T therapy responses. Indeed, by analysing different phenotypic profiles for several hematologic cancers and responses, we identified that the joint assessment of AUC0-28 and the corresponding fraction of non-exhausted CAR-T cells during the first 28 days after infusion may play an important role in the therapy outcome. The small number of patients used in this study poses a limitation that must be overcome by considering a larger cohort. Also, from the clinical point of view, the characterization of CAR-T phenotypes in patients still presents challenges due to a very few number of retrieved CAR-T cells. The follow-up samples after treatment are scarce in most cases, making it difficult the translation of data into the mathematical model difficult. Moreover, there is still a lot of discussion about the exhaustion markers in CAR-T cells [45].

CAR-T cell exhaustion is still a not fully understood factor that may limit the efficacy of the therapy. Exhausted CAR-T cell phenotype is characterized by an *in vivo* loss of functionality, expansion capacity, and persistence [45]. Thus, detecting the presence of exhausted cells and better understanding their onset and temporal evolution during the therapy can be key to improving results. Techniques to prevent, reverse, or delay the exhaustion process are currently under development [9,46,47]. Beider *et al.* [45] report that non-responding patients exhibit large amount of exhausted CAR-T cell phenotype. In addition, CAR-T cells from these patients presented functional impairment due to lower *in vitro* proliferative capacity and interleukin-2 production. Fraietta *et al.* [11] also report the greater exhaustion in non-responders, accompanied by low production of memory CAR-T cells. The results in the present work are in agreement with these findings.

There are cases in the literature reporting that the entire CAR-T cell population observed in a patient after injection derives from a single clone. This suggests that, in some cases, only a fraction of the injected CAR-T cells may engraft, survive, expand and generate memory [30,31]. Although our model does not explicitly consider the number of clones, we present some cases in which the population of effector CAR-T cells derives from the engraftment of only one or few CAR-T cell. This fact demonstrates the ability of our model to describe different scenarios, including the engraftment of ten to thousands of cells.

The distribution phase presents a variable duration in the different types of hematologic cancers. Liu *et al.* [22] highlight that patients with DLBCL have a well-marked distribution phase. In their model, the authors consider the existence of the distribution phase only when it is clearly indicated by the experimental data. In contrast, our model assumes that CAR-T cells go through the distribution phase soon after infusion regardless of the type of cancer. Thus, our model is able to represent distribution phases of different durations, from the shortest to the longest (patients with DLBCL). In any case, Huang *et al.* [2] highlight the need for a gradual reduction of the sampling frequency, with daily samples over the first days to capture the initial dynamics of CAR-T cells after infusion.

Regardless of the disease, CR patients exhibit diverse patterns of CAR-T cell expansion, ranging from the fastest and most intense to the least intense and most durable

 doi:10.20944/preprints202209.0359.v1

[37]. Fraietta *et al.* [11] reported a greater pool of memory CAR-T cells in CR patients. This memory pool formation pattern was not observed in our simulations. Some CR patients indeed exhibited great formation of memory cells while others had a very low percentage of this phenotype in the total CAR-T cell composition (see Figure 5). However, we have identified that all CR patients exhibit high fractions of non-exhausted CAR-T cells ($C_D + C_T + C_M$). In this way, a variety of dynamics was well represented by the developed model. This is particularly important with regard to the treatment exposure time reflected by the AUC0-28 parameter, which ultimately impacts the long-term therapy outcome. Patients P1 and P2, for example, exhibit high and low AUC0-28 values, respectively, while having low fractions of exhausted cells in the same period. Of note, these two patients represent a clinical milestone, being the first patients treated with CAR-T cell immunotherapy to remain cancer-free for a decade [5,48]. Our model simulations have captured those dynamics, with the presence of CAR-T cells in the blood during the ten years after infusion. By extending those simulation for additional ten years, our model predicts that patients P1 and P2 will remain cancer-free for at least another decade.

Assessing the long-term dynamics of each simulation fitted to patient data, we identified that some patients present sustained oscillations of CAR-T cells within the clinical undetectable region (see patient B12 in Figures SM-3 and SM-4, and patient P2 in Figure SM-5). This suggests the existence of a stable limit cycle for the ordinary differential equation (ODE) system, leading to period oscillations between CAR-T and tumor cells, always with values below clinically detectable levels. The mathematical analysis of the proposed model is underway in order to identify the conditions for the occurrence and stability properties of the observed cycles. Of note, the cyclic behavior in the range of measurable values is considered not biologically acceptable in [12] because it has never been observed clinically. However, Chong *et al.* [49] identified two long-term CR patients with CAR-T cells fluctuating between detectable and undetectable levels. Qi *et al.* [18] state that this fact may suggest possible existence of cycles in some patients.

Open-data sharing plays a critical role in the development of clinically useful mathematical models in many areas, including CAR-T immunotherapy. Together with open source software, they impact the potential of model development, bioanalytical methods, and designing methods to better inform the models with refined parameter values. Kast *et al.* [17] highlight the challenging task of building models that allow the identification of possible correlations between the various mechanisms present in the dynamics of CAR-T cells after infusion and the clinical responses in scenarios characterized by lack of data. We perform data collection and curation in different publications, often with limited access and incomplete information. Many publications still do not provide experimental data and information such as clinical quantification threshold, tumor burden after lymphodepletion and before CAR-T therapy, and therapy outcomes per patient. These still existing difficulties, when overcome, can significantly contribute to mathematical modeling and eventually benefit the advancement of cancer biology.

CAR-T cell immunotherapy presents great complexity inherent to the manufactured product and the heterogeneity between patients. We consider this variability into the model through the $\kappa(t)$ function. It directly describes patient-specific characteristics that interfere in the capacity and duration of expansion, and in the basal proliferation level of CAR-T cells. The heterogeneity of the infused product is also contemplated by this function implicitly. Note that our study involved different designs (CAR-T19 BBζ and CAR-T19 28ζ) and origins (autologous and allogeneic) of CAR-T cells as well as different dosing regimens (single and fractionated doses). The $\kappa(t)$ function was able to handle all the variability existing in these factors. As discussed by Liu *et al.* [22], these factors together with the product heterogeneity, patient responses, and disease types, also considered in the scenarios assessed here, may generate substantial variability in the kinetics of CAR-T cells. Therefore, in the results presented here, we have observed a

 doi:10.20944/preprints202209.0359.v1

great variability of the profiles of the $\kappa(t)$ function, allowing to describe the diversity of patient-specific patterns of antigen-dependent expansion. The review work presented in [2] identified some limitations of current mathematical models for describing adoptive cellular therapies in general. They mainly encompass not considering T cell heterogeneity (different phenotypes, subsets, and levels of exhaustiveness) and the role of tumor cells (antigen-expressing cells) in the different phases of T cell kinetics. With the focus on CAR-T cell therapy, Chaudhury *et al.* [12] also emphasized the importance of considering the phenotypic differentiation of both the infused product and those that eventually occur *in vivo* in the modeling. The model proposed here is able to circumvent those limitations. Qi *et al.* [18] emphasize the importance of developing models to describe the kinetics of CAR-T cells and their possible contributions to the identification of key parameters and their relationship with response to therapy. Overall, we hope that the proposed model may contribute to this development, generating insights into many challenges that still remain in CAR-T cell immunotherapy.

5. Conclusions

The kinetic profile of the CAR-T cell population in patients exhibit a great variability among patients and among diseases. The proposed multicompartment model encompassing CAR-T cell subpoppulations of functional, memory, and exhausted cells was able to capture the dynamics of the therapy regardless of the such variability. Further, the observation of some parameters of the CAR-T cell phenotypic dynamics and therapy outcomes suggest that the joint assessment of the AUC0-28 and the corresponding fraction of non-exhausted CAR-T cells has the potential to be used as a predictive marker of the long-term response to CAR-T immunotherapy. The expansion of the study presented here involving a larger cohort will enhance the understanding of the variability in patient-specific treatment responses.

Supplementary Materials: The Supplementary Material shows details about the experimental data obtained and unit transformations, describes the method used for calibrating the model, provides the fits obtained in the linear scale for all patients and the corresponding parameter values used in the final simulations, and present the values of the cellular kinetic parameters that were used to establish relation with patient responses

Author Contributions: Conceptualization, E.A.P., L.R.C.B., A.C.F., and R.C.A.; methodology, E.A.P., A.C.F., and R.C.A.; code development and experiment execution, E.A.P.; manuscript draft preparation, E.A.P., L.R.C.B., A.C.F., and R.C.A. All authors have read and agreed to the published version of the manuscript.

Funding: This research was funded by Conselho Nacional de Desenvolvimento Científico e Tecnológico (CNPq) and Coordenação de Aperfeiçoamento de Pessoal de Nível Superior (CAPES).

Institutional Review Board Statement: Not applicable

Data Availability Statement: Source data are provided in this paper and all data used in this study can be downloaded from the cited sources. All information, as parameters values, to replicate simulations and analysis are available in this work.

Conflicts of Interest: The authors declare no conflicts of interest.

Abbreviations

The following abbreviations are used in this manuscript:

CAR	Chimeric antigen receptor
ALL	Acute lymphoblastic leukemia
MCL	Mantle cell lymphoma
DLBCL	Diffuse large B cell lymphoma
BCMA	B cell maturation antigen
HST	Hair Stem Cell Transplantation
PB	Peripheral blood
BM	Bone marrow
ODE	Ordinary differential equation
CR	Complete response
PR	Partial response
SD	Stable disease
PD	Progressive disease
IDO	Indoleamine 2,3-dioxygenase

References

1. Barros, L.R.C.; Couto, S.C.F.; da Silva Santurio, D.; Paixão, E.A.; Cardoso, F.; da Silva, V.J.; Klinger, P.; Ribeiro, P.d.A.C.; Rós, F.A.; Oliveira, T.G.M.; Rego, E.M.; Ramos, R.N.; Rocha, V. Systematic Review of Available CAR-T Cell Trials around the World. *Cancers* **2022**, *14*, 2667. doi:10.3390/cancers14112667.
2. Huang, W.; Li, J.; Liao, M.Z.; Liu, S.N.; Yu, J.; Jing, J.; Kotani, N.; Kamen, L.; Guelman, S.; Miles, D.R. Clinical Pharmacology Perspectives for Adoptive Cell Therapies in Oncology. *Clinical Pharmacology & Therapeutics* **2022**, *n/a*, 1–14. doi:10.1002/cpt.2509.
3. Lee, D.W.; Kochenderfer, J.N.; Stetler-Stevenson, M.; Cui, Y.K.; Delbrook, C.; Feldman, S.A.; Fry, T.J.; Orentas, R.; Sabatino, M.; Shah, N.N.; Steinberg, S.M.; Stroncek, D.; Tschernia, N.; Yuan, C.; Zhang, H.; Zhang, L.; Rosenberg, S.A.; Wayne, A.S.; Mackall, C.L. T cells expressing CD19 chimeric antigen receptors for acute lymphoblastic leukaemia in children and young adults: a phase 1 dose-escalation trial. *Lancet* **2015**, *385*, 517–528. doi:10.1016/S0140-6736(14)61403-3.
4. Shah, N.N.; Lee, D.W.; Yates, B.; Yuan, C.M.; Shalabi, H.; Martin, S.; Wolters, P.L.; Steinberg, S.M.; Baker, E.H.; Delbrook, C.P.; Stetler-Stevenson, M.; Fry, T.J.; Stroncek, D.F.; Mackall, C.L. Long-Term Follow-Up of CD19-CAR T-Cell Therapy in Children and Young Adults With B-ALL. *Journal of Clinical Oncology* **2021**, *39*, 1650–1659. PMID: 33764809, doi:10.1200/JCO.20.02262.
5. Melenhorst, J.J.; Chen, G.M.; Wang, M.; Porter, D.L.; Chen, C.; Collins, M.A.; Gao, P.; Bandyopadhyay, S.; Sun, H.; Zhao, Z.; Lundh, S.; Pruteanu-Malinici, I.; Nobles, C.L.; Maji, S.; Frey, N.V.; Gill, S.I.; Tian, L.; Kulikovskaya, I.; Gupta, M.; Ambrose, D.E.; Davis, M.M.; Fraietta, J.A.; Brogdon, J.L.; Young, R.M.; Chew, A.; Levine, B.L.; Siegel, D.L.; Alanio, C.; Wherry, E.J.; Bushman, F.D.; Lacey, S.F.; Tan, K.; June, C.H. Decade-long leukaemia remissions with persistence of CD4+ CAR T cells. *Nature* **2022**, *602*, 1476–4687. doi:10.1038/s41586-021-04390-6.
6. Gardner, R.A.; Finney, O.; Annesley, C.; Brakke, H.; Summers, C.; Leger, K.; Bleakley, M.; Brown, C.; Mgebroff, S.; Kelly-Spratt, K.S.; Hoglund, V.; Lindgren, C.; Oron, A.P.; Li, D.; Riddell, S.R.; Park, J.R.; Jensen, M.C. Intent-to-treat leukemia remission by CD19 CAR T cells of defined formulation and dose in children and young adults. *Blood* **2017**, *129*, 3322–3331, [https://ashpublications.org/blood/article-pdf/129/25/3322/1364282/blood769208.pdf]. doi:10.1182/blood-2017-02-769208.
7. Poorebrahim, M.; Melief, J.; de Coaña, Y.P.; Wickström, S.L.; Cid-Arregui, A.; Kiessling, R. Counteracting CAR T cell dysfunction. *Oncogene* **2021**, *40*, 421 – 435. doi:10.1038/s41388-020-01501-x.
8. Shah, N.N.; Fry, T.J. Mechanisms of resistance to CAR T cell therapy. *Nature Reviews Clinical Oncology* **2019**, *16*, 372–385. doi:10.1038/s41571-019-0184-6.
9. Larson, R.C.; Maus, M.V. Recent advances and discoveries in the mechanisms and functions of CAR T cells. *Nature Reviews Cancer* **2021**, *21*, 145–161. doi:10.1038/s41568-020-00323-z.
10. Eyquem, J.; Mansilla-Soto, J.; Giavridis, T.; van der Stegen, S.; Hamieh, M.; Cunanan, K.; Odak, A.; Gönen, M.; Sadelain, M. Targeting a CAR to the TRAC locus with CRISPR/Cas9 enhances tumour rejection. *Nature* **2017**, *543*, 113 – 117. doi:10.1038/nature21405.
11. Fraietta, J.; Lacey, S.; Orlando, E.; Pruteanu-Malinici, I.; Gohil, M.; Lundh, S.; Boesteanu, A.; Wang, Y.; O'Connor, R.; Hwang, W.T.; Pequignot, E.; Ambrose, D.; Zhang, C.; Wilcox, N.; Bedoya, F.; Dorfmeier, C.; Chen, F.; Tian, L.; Parakandi, H.; Gupta, M.; Young, R.; Johnson, F.; Kulikovskaya, I.; Liu, L.; Xu, J.; Kassim, S.; Davis, M.; Levine, B.; Frey, N.; Siegel, D.; Huang, A.; Wherry, E.; Bitter, H.; Brogdon, J.; Porter, D.; June, C.; Melenhorst, J. Determinants of response and resistance to CD19 chimeric antigen receptor (CAR) T cell therapy of chronic lymphocytic leukemia. *Nature Medicine* **2018**, *24*, 563–571. doi:10.1038/s41591-018-0010-1.
12. Chaudhury, A.; Zhu, X.; Chu, L.; Goliaei, A.; June, C.; Kearns, J.; Stein, A. Chimeric Antigen Receptor T Cell Therapies: A Review of Cellular Kinetic-Pharmacodynamic Modeling Approaches. *Journal of Clinical Pharmacology* **2020**, *60*, S147–S159. doi:10.1002/jcph.1691.
13. Pillai, V.; Muralidharan, K.; Meng, W.; Bagashev, A.; Oldridge, D.A.; Rosenthal, J.; Arnam, J.V.; Melenhorst, J.J.; Mohan, D.; DiNofia, A.M.; Luo, M.; Cherian, S.; Fromm, J.R.; Wertheim, G.; Thomas-Tikhonenko, A.; Paessler, M.; June, C.H.; Prak, E.T.L.; Bhoj, V.G.; Grupp, S.A.; Maude, S.L.; Rheingold, S.R. CAR T-cell therapy is effective for CD19-dim B-lymphoblastic leukemia but is impacted by prior blinatumomab therapy. *Blood Advances* **2019**, *3*, 3539 – 3549. doi:10.1182/bloodadvances.2019000692.
14. Ghorashian, S.; Kramer, A.M.; Onuoha, S.; G., W.; others. Enhanced CAR T cell expansion and prolonged persistence in pediatric patients with ALL treated with a low-affinity CD19 CAR. *Nature Medicine* **2019**, *25*, 1408 – 1414. doi:10.1038/s41591-019-0549-5.

15. Xu, X.; Huang, S.; Xiao, X.; Sun, Q.; Liang, X.; Chen, S.; Zhao, Z.; Huo, Z.; Tu, S.; Li, Y. Challenges and Clinical Strategies of CAR T-Cell Therapy for Acute Lymphoblastic Leukemia: Overview and Developments. *Frontiers in Immunology* **2021**, *11*, 569117. doi:10.3389/fimmu.2020.569117.
16. Nukala, U.; Messan, M.R.; Yogurtcu, O.N.; Wang, X.; Yang, H. A Systematic Review of the Efforts and Hindrances of Modeling and Simulation of CAR T-cell Therapy. *The AAPS Journal* **2021**, *23*, 52. doi:10.1208/s12248-021-00579-9.
17. Kast, J.; Nozohouri, S.; Zhou, D.; Yago, M.R.; Chen, P.W.; Ahamadi, M.; Dutta, S.; Upreti, V.V. Recent advances and clinical pharmacology aspects of Chimeric Antigen Receptor (CAR) T-cellular therapy development. *Clinical Translational Science* **2022**, *00*, 1–18. doi:10.1111/cts.13349.
18. Qi, T.; McGrath, K.; Ranganathan, R.; Dotti, G.; Cao, Y. Cellular kinetics: A clinical and computational review of CAR-T cell pharmacology. *Advanced Drug Delivery Reviews* **2022**, *188*, 114421. doi:10.1016/j.addr.2022.114421.
19. Arya, V.; Venkatakrishnan, K. Role of Physiologically Based Pharmacokinetic Modeling and Simulation in Enabling Model-Informed Development of Drugs and Biotherapeutics. *The Journal of Clinical Pharmacology* **2020**, *60*, S7–S11. doi:10.1002/jcph.1770.
20. Mueller, K.; Maude, S.; Porter, D.; Frey, N.; Wood, P.; Han, X.; Waldron, E.; Chakraborty, A.; Awasthi, R.; Levine, B.; Melenhorst, J.; Grupp, S.; June, C.; Lacey, S. Cellular kinetics of CTL019 in relapsed/refractory B-cell acute lymphoblastic leukemia and chronic lymphocytic leukemia. *Blood* **2017**, *130*, 2317–2325. doi:10.1182/blood-2017-06-786129.
21. Stein, A.M.; Grupp, S.A.; Levine, J.E.; Laetsch, T.W.; Pulsipher, M.A.; Boyer, M.W.; August, K.J.; Levine, B.L.; Tomassian, L.; Shah, S.; Leung, M.; Huang, P.H.; Awasthi, R.; Mueller, K.T.; Wood, P.A.; June, C.H. Tisagenlecleucel Model-Based Cellular Kinetic Analysis of Chimeric Antigen Receptor–T Cells. *CPT: Pharmacometrics & Systems Pharmacology* **2019**, *8*, 285–295. doi:10.1002/psp4.12388.
22. Liu, C.; Ayyar, V.S.; Zheng, X.; Chen, W.; Zheng, S.; Mody, H.; Wang, W.; Heald, D.; Singh, A.P.; Cao, Y. Model-Based Cellular Kinetic Analysis of Chimeric Antigen Receptor-T Cells in Humans. *Clinical Pharmacology & Therapeutics* **2021**, *109*, 716–727. doi:10.1002/cpt.2040.
23. Singh, A.P.; Chen, W.; Zheng, X.; Mody, H.; Carpenter, T.J.; Zong, A.; Heald, D.L. Bench-to-bedside translation of chimeric antigen receptor (CAR) T cells using a multiscale systems pharmacokinetic-pharmacodynamic model: A case study with anti-BCMA CAR-T. *CPT: Pharmacometrics & Systems Pharmacology* **2021**, *10*, 362–376. doi:10.1002/psp4.12598.
24. Singh, A.P.; Zheng, X.; Lin-Schmidt, X.; Chen, W.; Carpenter, T.J.; Zong, A.; Wang, W.; Heald, D.L. Development of a quantitative relationship between CAR-affinity, antigen abundance, tumor cell depletion and CAR-T cell expansion using a multiscale systems PK-PD model. *mAbs* **2020**, *12*, 1688616. doi:10.1080/19420862.2019.1688616.
25. Kimmel, G.J.; Locke, F.L.; Altrock, P.M. The roles of T cell competition and stochastic extinction events in chimeric antigen receptor T cell therapy. *Proceedings of The Royal Society B* **2021**, *288*, 20210229. doi:10.1098/rspb.2021.0229.
26. Owens, K.; Bozic, I. Modeling CAR T-Cell Therapy with Patient Preconditioning. *Bulletin of Mathematical Biology* **2021**, *83*, 42–36. doi:10.1007/s11538-021-00869-5.
27. Hardiansyah, D.; Ng, C.M. Quantitative Systems Pharmacology Model of Chimeric Antigen Receptor T-Cell Therapy. *Clinical Translational Science* **2019**, *12*, 343–349. doi:10.1111/cts.12636.
28. Barros, L.R.C.; Paixão, E.A.; Valli, A.M.P.; Naozuka, G.T.; Fassoni, A.C.; Almeida, R.C. CARTmath—A Mathematical Model of CAR-T Immunotherapy in Preclinical Studies of Hematological Cancers. *Cancers* **2021**, *13*, 2941. doi:10.3390/cancers13122941.
29. Sheih, A.; Voillet, V.; Hanafi, L.A.; DeBerg, H.A.; Yajima, M.; Hawkins, R.; Gersuk, V.; Riddell, S.R.; Maloney, D.G.; Wohlfahrt, M.E.; Pande, D.; Enstrom, M.R.; Kiem, H.P.; Adair, J.E.; Gottardo, R.; Linsley, P.S.; Turtle, C.J. Clonal kinetics and single-cell transcriptional profiling of CAR-T cells in patients undergoing CD19 CAR-T immunotherapy. *Nature Communications* **2020**, *11*, 219. doi:10.1038/s41467-019-13880-1.
30. Fraietta, J.A.; Nobles, C.L.; Sammons, M.A.; Lundh, S.; Carty, S.A.; Reich, T.J.; Cogdill, A.P.; Morrissette, J.J.D.; DeNizio, J.E.; Reddy, S.; Hwang, Y.; Gohil, M.; Kulikovskaya, I.; Nazimuddin, F.; Gupta, M.; Chen, F.; Everett, J.K.; Alexander, K.A.; Lin-Shiao, E.; Gee, M.H.; Liu, X.; Young, R.M.; Ambrose, D.; Wang, Y.; Xu, J.; Jordan, M.S.; Marcucci, K.T.; Levine, B.L.; Garcia, K.C.; Zhao, Y.; Kalos, M.; Porter, D.L.; Kohli, R.M.; Lacey, S.F.; Berger, S.L.; Bushman, F.D.; June, C.H.; Melenhorst, J.J. Disruption of TET2 promotes the therapeutic efficacy of CD19-targeted T cells. *Nature* **2018**, *558*, 307–312. doi:10.1038/s41586-018-0178-z.
31. Shah, N.; Qin, H.; Yates, B.; Su, L.; Shalabi, H.; Raffeld, M.; Ahlman, M.; Stetler-Stevenson, M.; Yuan, C.; Guo, S.; Liu, S.; Hughes, S.; Fry, T.; Wu, X. Clonal expansion of CAR T cells harboring lentivector integration in the CBL gene following anti-CD22 CAR T-cell therapy. *Blood Advances* **2019**, *3*, 2317–2322. doi:10.1182/bloodadvances.2019000219.
32. Kimmel, G.J.; Locke, F.L.; Altrock, P.M. The roles of T cell competition and stochastic extinction events in chimeric antigen receptor T cell therapy. *Proceedings of the Royal Society B* **2021**, *288*, 20210229. doi:10.1098/rspb.2021.0229.
33. Ninomiya, S.; Narala, N.; Huye, L.; Yagyu, S.; Savoldo, B.; Dotti, G.; Heslop, H.E.; Brenner, M.K.; Rooney, C.M.; Ramos, C.A. Tumor indoleamine 2, 3-dioxygenase (IDO) inhibits CD19-CAR T cells and is downregulated by lymphodepleting drugs. *Blood* **2015**, pp. 3905 – 3916. doi:10.1182/blood-2015-01-621474.
34. De Boer, R.J.; Perelson, A.S. Quantifying T lymphocyte turnover. *Journal of Theoretical Biology* **2013**, *327*, 45–87. doi:10.1016/j.jtbi.2012.12.025.
35. de Pillis, L.G.; Radunskaya, A.E.; Wiseman, C.L. A Validated Mathematical Model of Cell-Mediated Immune Response to Tumor Growth. *Cancer Research* **2005**, *65*, 7950–7958. doi:10.1158/0008-5472.CAN-05-0564.
36. Robertson-Tessi, M.; El-Kareh, A.; Goriely, A. A mathematical model of tumor–immune interactions. *Journal of Theoretical Biology* **2012**, *294*, 56–73. doi:10.1016/j.jtbi.2011.10.027.

37. Brudno, J.N.; Somerville, R.P.; Shi, V.; Rose, J.J.; Halverson, D.C.; Fowler, D.H.; Gea-Banacloche, J.C.; Pavletic, S.Z.; Hickstein, D.D.; Lu, T.L.; Feldman, S.A.; Iwamoto, A.T.; Kurlander, R.; Maric, I.; Goy, A.; Hansen, B.G.; Wilder, J.S.; Blacklock-Schuver, B.; Hakim, F.T.; Rosenberg, S.A.; Gress, R.E.; Kochenderfer, J.N. Allogeneic T Cells That Express an Anti-CD19 Chimeric Antigen Receptor Induce Remissions of B-Cell Malignancies That Progress After Allogeneic Hematopoietic Stem-Cell Transplantation Without Causing Graft-Versus-Host Disease. *Journal of Clinical Oncology* **2016**, *34*, 1112–1121. doi:10.1200/JCO.2015.64.5929.
38. Porter, D.L.; Hwang, W.T.; Frey, N.V.; Lacey, S.F.; Shaw, P.A.; Loren, A.W.; Bagg, A.; Marcucci, K.T.; Shen, A.; Gonzalez, V.; Ambrose, D.; Grupp, S.A.; Chew, A.; Zheng, Z.; Milone, M.C.; Levine, B.L.; Melenhorst, J.J.; June, C.H. Chimeric antigen receptor T cells persist and induce sustained remissions in relapsed refractory chronic lymphocytic leukemia. *Science Translational Medicine* **2015**, *7*, 303ra139–303ra139, [https://www.science.org/doi/pdf/10.1126/scitranslmed.aac5415]. doi:10.1126/scitranslmed.aac5415.
39. Rohatgi, A. WebPlotDigitizer, 2020. Version 4.5. Available at https://apps.automeris.io/wpd/.
40. Cheson, B.; Pfistner, B.; Juweid, M.; Gascoyne, R.; Specht, L.; Horning, S.; Coiffier, B.; Fisher, R.; Hagenbeek, A.; Zucca, E.; Rosen, S.; Stroobants, S.; Lister, T.; Hoppe, R.; Dreyling, M.; Tobinai, K.; Vose, J.; Connors, J.; Federico, M.; Diehl, V. International Harmonization Project on Lymphoma: Revised response criteria for malignant lymphoma. *Journal of Clinical Oncology* **2007**, *25*, 579–586. doi:10.1200/JCO.2006.09.2403.
41. Hallek, M.; Cheson, B.D.; Catovsky, D.; Caligaris-Cappio, F.; Dighiero, G.; Döhner, H.; Hillmen, P.; Keating, M.J.; Montserrat, E.; Rai, K.R.; Kipps, T.J. Guidelines for the diagnosis and treatment of chronic lymphocytic leukemia: a report from the International Workshop on Chronic Lymphocytic Leukemia updating the National Cancer Institute–Working Group 1996 guidelines. *Blood* **2008**, *111*, 5446–5456, [https://ashpublications.org/blood/article-pdf/111/12/5446/1298113/zh802508005446.pdf]. doi:10.1182/blood-2007-06-093906.
42. Faires, J.D.; Burden, R.L. *Numerical Methods*; Cengage Learning: Belmont, CA, USA, 2003.
43. Ogasawara, K.; Dodds, M.; Mack, T.; Lymp, J.; Dell'Aringa, J.; Smith, J. Population Cellular Kinetics of Lisocabtagene Maraleucel, an Autologous CD19-Directed Chimeric Antigen Receptor T-Cell Product, in Patients with Relapsed/Refractory Large B-Cell Lymphoma. *Clinical Pharmacokinetics* **2021**, *60*, 1621–1633. doi:10.1007/s40262-021-01039-5.
44. Maude, S.L.; Laetsch, T.W.; Buechner, J.; Rives, S.; Boyer, M.; Bittencourt, H.; Bader, P.; Verneris, M.R.; Stefanski, H.E.; Myers, G.D.; Qayed, M.; De Moerloose, B.; Hiramatsu, H.; Schlis, K.; Davis, K.L.; Martin, P.L.; Nemecek, E.R.; Yanik, G.A.; Peters, C.; Baruchel, A.; Boissel, N.; Mechinaud, F.; Balduzzi, A.; Krueger, J.; June, C.H.; Levine, B.L.; Wood, P.; Taran, T.; Leung, M.; Mueller, K.T.; Zhang, Y.; Sen, K.; Lebwohl, D.; Pulsipher, M.A.; Grupp, S.A. Tisagenlecleucel in Children and Young Adults with B-Cell Lymphoblastic Leukemia. *New England Journal of Medicine* **2018**, *378*, 439 – 448. PMID: 29385370, doi:10.1056/NEJMoa1709866.
45. Beider, K.; Itzhaki, O.; Schachter, J.; Grushchenko-Polaq, A.; Voevoda-Dimenshtein, V.; Rosenberg, E.; Ostrovsky, O.; Devillers, O.; Frommer, R.; Zeltzer, L.; Toren, A.; Jacoby, E.; Shimoni, A.; Avigdor, A.; Nagler, A.; Besser, M. Molecular and Functional Signatures Associated with CAR T Cell Exhaustion and Impaired Clinical Response in Patients with B Cell Malignancies. *Cells* **2022**, *11*, 1140. doi:10.3390/cells11071140.
46. Poorebrahim, M.; Melief, J.; de Coaña, Y.P.; Wickström, S.L.; Cid-Arregui, A.; Kiessling, R. Counteracting CAR T cell dysfunction. *Oncogene* **2021**, *40*, 421 – 435. doi:10.1038/s41388-020-01501-x.
47. Lynn, R.C.; Weber, E.W.; Sotillo, E.; Gennert, D.; Xu, P.; Good, Z.; Anbunathan, H.; Lattin, J.; Jones, R.; Tieu, V.; Nagaraja, S.; Granja, J.; de Bourcy, C.F.A.; Majzner, R.; Satpathy, A.T.; Quake, S.R.; Monje, M.; Chang, H.Y.; Mackall, C.L. c-Jun overexpression in CAR T cells induces exhaustion resistance. *Nature* **2019**, *576*, 293–300. doi:10.1038/s41586-019-1805-z.
48. Maus, M.V. A decade of CAR T cell evolution. *Nature Cancer* **2022**, *3*, 270–271. doi:10.1038/s43018-022-00347-4.
49. Chong, E.A.; Ruella, M.; Schuster, S.J. Five-Year Outcomes for Refractory B-Cell Lymphomas with CAR T-Cell Therapy. *New England Journal of Medicine* **2021**, *384*, 673–674. PMID: 33596362, doi:10.1056/NEJMc2030164.